2

What is the Pulsed Cathodoluminescence?

Vladimir Solomonov and Alfiya Spirina
The Institute of Electrophysics of Ural Branch of the Russian Academy of Sciences
Russia

1. Introduction

A cathodoluminescence phenomenon was revealed in the 19th century. The first explanation of this phenomenon was given by Julius Plücker in 1858, and two decades later by Sir William Crookes (1879). A cathodoluminescence intensity is defined by the concentration of electrons (holes) – $n_{e(h)}$, generated by electrons injected into substance. Generally, this concentration is described by the kinetic equation

$$\frac{dn_{e(h)}}{dt} = G - An_{e(h)} - Bn_{e(h)}^2 , \quad G = \frac{E_0 j_e}{ed_e \varepsilon_i} . \tag{1}$$

Here A and B are the coefficients of electrons (holes) recombination processes which obey to linear and quadratic laws. Coefficient A is a generalized characteristic of the processes which relate to formation and dissociation of electron and hole centres. These processes are accompanied with the capture or the release of free electron (hole). The luminescence intensity of these centres is proportional to concentration, $I_{e(h)} \sim A \cdot n_{e(h)}$. Coefficient B is defined by the annihilation of free electron-hole pairs which resulted in origination of interband, excitonic, and intracentre kinds of luminescence with intensity of $I \sim B \cdot n^2_{e(h)}$. Thus, the coefficients A and B are the characteristics of certain substance. Usually for pure crystals (undoped) the coefficient A has an order of 10^5-10^6 s^{-1} whereas it is of 10^8 s^{-1} in case of crystals doped with donor (acceptor) ions. The value of coefficient B amounts to 10^{-10} $cm^3 \cdot s^{-1}$ for the interband transition in large-band-gap semiconductors [Bogdankevich et al., 1975, Galkin, 1981]. Coefficient G is the generation rate of electron-hole pairs inside a sample that is irradiated by primary electrons. The energy and current density of these electrons are determined as follows

$$E_0 = eU_0 , j_e = \frac{i_e}{S} . \tag{2}$$

In Eqs. (1) and (2) U_0, e, i_e, S, d_e are an accelerating potential, electron charge, a current of accelerated electrons, an irradiated area of sample and an electron penetration depth, respectively. An average ionization energy ε_i in Eq. (1) can be approximately estimated as $\varepsilon_i \approx 3 \cdot E_g$, where E_g is a band-gap energy.

The current of accelerated electrons (i_e), being injected into the sample, can be determined with the help of equivalent circuit that is shown in Fig. 1.

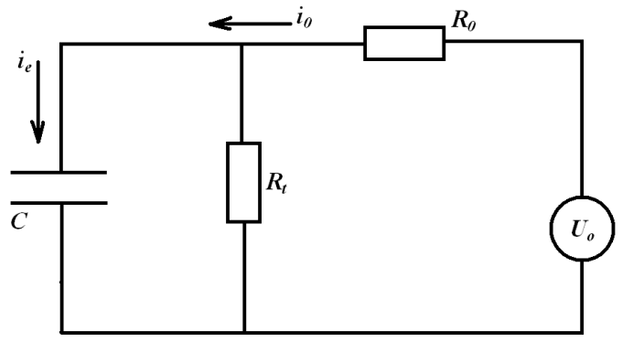

Fig. 1. The equivalent circuit of electron current

Here electron accelerator is represented as a source of accelerating potential U_0 with internal resistance $R_0=U_0/i_0=$const. The sample with irradiated surface $S=\pi r_0^2$ forms a capacitor with $C=2\pi r_0 \varepsilon \varepsilon_0$. Here ε_0 is the dielectric constant and ε is the permittivity of environment (e.g. air). Resistor R_t is introduced as a shunt for capacitor C and it provides the discharge of the sample surface. For this circuit at $R_t=$const and initial condition $i_e(0)=i_o$, the electron current is described by the equation

$$i_e(t)=\frac{U_0}{R_0+R_t}\left[1-\exp\left(-\frac{t}{\tau_c}\right)\right]+i_{e0}\exp\left(-\frac{t}{\tau_c}\right), \tag{3}$$

where $\tau_c=CR_0R_t/(R_0+R_t)$ is a typical charge time of capacity C.

For example, in the cathodoluminescent microscope [Ramseyer et. al., 1989, Petrov, 1996] the shunting of capacity C is provided by the emission of secondary electrons over the irradiated sample surface. This emission results in setting the finite value of shunting resistance R_t. Dynamic balance between the primary electrons which are injected into the sample, and the secondary electrons which leave the sample is equilibrated at $t>>\tau_c$. After that time the current of injected electrons i_e tends to achieve the value defined as $i_e=U_0/(R_0+R_t)$ and the constant generation rate of electron-hole pairs G is equilibrated. These conditions are realized for the narrow energy range of the primary electrons $1<E_e<12$ keV resulted in a small depth of electron penetration $d_e=0.1$-1.5 μm. Thus, the lower energy of the primary electrons is limited by the work function of the secondary electrons through the sample surface. The upper one is limited by the energy loss of secondary electrons, which appeared on the large depth inside the sample, under diffusion to the sample surface.

The solution of Eq. (1) using G=const reveals that under irradiation by electron beam the concentration of electron-hole pairs inside the sample volume which is determined by the beam cross-section and penetration depth of electrons is saturated rapidly with time according to the following equation:

$$n_{e(h)}=2G\tau_i\frac{\exp(t/\tau_i)-1}{\delta\exp(t/\tau_i)+\gamma}\xrightarrow{t\to\infty}2G\frac{\tau_i}{1+A\tau_i},\tau_i=\frac{1}{\sqrt{4BG+A^2}}. \tag{4}$$

Here τ_i is an ionization time of substance, $\delta=1+A\tau_i$, $\gamma=1-A\tau_i$, where $A\tau_i<1$. From the Eq. (4) it can be seen that the concentration of electron-hole pairs increases with increasing the

coefficient G. Therefore in order to achieve a high brightness of luminescence, the electron beam is focused on the sample surface in the spot with a diameter of 1-50 μm and current density j_e in the range from 10^{-2} to 10 A/cm^2. The coefficient G amounts to 10^{23}-10^{26} cm^{-3}·s^{-1} and the range of typical time τ_i has an order of 10^{-6}-10^{-9} s.

Since the 1980-s the electron beams with the energy increased to 20-70 keV and density of electron current of j_e=0.1-10 A/cm^2 are applied. These electrons are able to penetrate into the sample on a depth of 3-30 μm [Chukichev et. al., 1990, Yang et. al., 1992]. The secondary electrons originated on such a depth inside the sample dissipate their own energy while moved to the outer surface and can't emit outside. In this case the dynamic balance is provided by the flow of the surplus charge via thin metal film previously deposited on the sample surface being irradiated and served as a ground. Now the shunt R_t is determined by the contact electroconductivity of the irradiated area with the metal film. At these parameters of electron beam the coefficient G, the ionization time τ_i and the charging time of capacity τ_c have values of the same order those were mentioned above. However, at increased energy of electrons the luminescence intensity increases due to the deeper penetration of electrons and as a result the larger excited volume of substance.

To decrease the thermal load on the irradiated surface at the electron energy of 20-70 keV the pulsed electron beam with the pulse duration of 1-10 ms [Chukichev et. al., 1990] or modulated electron beam with the modulation frequency of 100-300 Hz [Yang et. al., 1992] are applied. The luminescence, excited by such electron beams, is usually called the pulsed cathodoluminescence (PCL) [Chukichev et. al., 1990]. However, this PCL is the steady-state one since the pulse duration of injected electrons is much greater than τ_i and τ_c yet.

PCL [Solomonov et. al., 2003], to be talked about in the present chapter, is excited at the conditions when the dynamic balance between the injected and left electrons is absent, i.e. at $R_t \to \infty$. The Eq. (3) shows in this case that the current of injected electrons damps exponentially with characteristic time constant τ_v, as

$$i_e(t) = i_{eo} \exp(-t / \tau_v), \quad \tau_v = R_0 C = \frac{2\varepsilon\varepsilon_0 U_0}{j_{e0} r_0}. \tag{5}$$

This time, τ_v, increases with energy of injected electrons. Its value is about 3.5 ns at E_0=200 keV, j_{e0}=100 A/cm^2, r_0=1 mm, and ε=1 according to Eq. (5). Therefore the PCL excitation should be carried out by the electron beam with duration t_e of the same order as τ_v. The electrons with energy of 100-200 keV penetrate into dielectric solids on the depth of 100-150 μm. Due to the large penetration depth the coefficient G reaches the value of 10^{26}-10^{27} cm^{-3}·s^{-1}, which is similar to that realized at maximum excitation conditions of the steady-state cathodoluminescence. When $t_e \le \tau_v$ the concentration of electron-hole pairs comes to $n_{e(h)} \ge 0.5 n_{e(h)max}$ according to Eq. (4). Here $n_{e(h)max}$ is a maximal value of the concentration at $t_e \to \infty$. It means that PCL brightness is higher than that of steady-state cathodoluminescence excited at the maximal conditions.

PCL spectrum gives the information about the composition and crystal structure of the sample bulk rather than interface layer. Interface layers are usually characterized with presence of many absorbed molecules and defect of crystal structure and their properties are not inherent to the bulk of materials. In PCL the interface layers with a thickness up to 20 μm don't have a significant influence on the PCL spectrum quality [Ramseyer et. al., 1990].

It should be emphasized that despite of short time of electron beam impact PCL persistence occurs and its kinetics is ascribed by complicated laws. This is associated with that the primary source of luminescence excitation is the electron-hole pairs. Their concentration according to Eq. (1) over the time of electron beam impact (G=0) is given by

$$n_{e(h)} = \frac{A}{B} \cdot \frac{\alpha \cdot \exp(-At)}{1 - \alpha \cdot \exp(-At)}, \alpha = \frac{B \cdot n_{eh0}}{A + B \cdot n_{eh0}}. \quad (6)$$

Here n_{eh0} is the concentration of electron-hole pairs introduced by the electron beam. The luminescence intensity of the electron and hole centres changes the same law. The intensity of interband luminescence falls proportionally to n^2_{eh}. These kinds of luminescence reach their maxima at the time moment when the excitation is over. The intensity of intracentre luminescence changes more difficulty. The first maximum is also reached at the same time moment but further behaviour depends on the life time of radiative level (τ_r). In the paper [Solomonov et. al., 1996, 2003] it has been shown that there is the second maximum of the intensity in the long persistence at $\tau_r > (\sqrt{2} - 1)/A$. After this maximum the intensity falls according to the exponential law with the characteristic time constant τ_r. Moreover the second maximum can be more intensive than the first one. If the $\tau_r < (\sqrt{2} - 1)/A$ the second maximum doesn't appear and an exponential decay of luminescence occurs but with characteristic time constant that is proportional to 1/(2A). It is worthy to note that in case of using nanosecond exciting electron beams the integral intensity of persistent luminescence is usually similar or even higher than that during excitation.

2. Apparatus for the PCL registration

The generation of high-current nanosecond electron beam with the energy higher than 100 keV became possible after creation of electron accelerators by G.A. Mesyats in the 1970-s. These accelerators are founded on the explosive electron emission [Mesyats, 1974]. The electrons having this energy extend at great distance (more than 10 cm) in air. The samples excited in air can be used in the form of pieces, powders, and solution. The irradiation in air furthers also to the partial compensation of injected charge into sample by the stream of positive air ions, created by the electron beam. The large penetration depth of these electrons into sample simplifies the sample preparation for analysis considerably, namely there is no need to undergo the sample to grinding and polishing procedures. Moreover irradiated surface doesn't require metallization. This is very important for the analysis of the finished product, in particular, jewels. It should be also noted that the problem of sample warming, which is typical for the steady-state cathodoluminescence, is solved due to the introduction of the small energy density (≤ 3 J/cm^3).

The investigation of PCL in the different mediums has shown that the portable nanosecond accelerators of RADAN [Mesyats et. al., 1992] are most applicable for its excitation. These accelerators include the sealed vacuum electron tube. The biological shielding from X-ray emission is provided by the design of analytic chamber, which is connected with the output of the accelerator. The analysed samples are placed into the chamber. The pulsed type of the luminescence allows using the different methods of its registration.

As a first, the traditional method of the registration with the help of optical monochromator, photoelectronic multiplier, and oscillograph is applied [Vaysburd et.al., 1982, Solomonov et. al., 1996]. The intensity kinetics of separated luminescence band is measured by this method. This is necessary for the identification of its nature. The application of the scanning monochromator allows registering the intensity distribution by wavelengths I (λ,t). However, two PCL features have to be kept in mind. The first feature is that the PCL is characterised by the certain degree of instability of the registered parameters because of the pulsed regime. Therefore the spectrum measurement has to be performed in the averaging mode. The second feature is caused by the different kinetics of PCL bands with the various nature and spectrum registered by such an approach strongly depends on time.

As a second, the time-integral intensity of the luminescent bands can be measured

$$I(\lambda) = \int_{t_1}^{t_2} I(\lambda, t)dt \ . \tag{7}$$

Here I (λ,t) is the current intensity, t_1 is the beginning of registration and t_2 is the ending of registration. This intensity is registered with the help of multichannel semiconductor photodetectors based on diode matrix and charge-coupled device [Solomonov et. al., 2003]. In this case optical spectrograph is applied instead of the scanning monochromator and the wide spectral range for one frame is measured. This method can be used for the PCL research when intracentre luminescence is dominant. Also the kinetic information about all registered spectrum can be obtained by means of changing of the integration limits t_1 and t_2.

Fig. 2 demonstrates the scheme of experimental setup for the receiving of PCL spectra. The setup consists of the luminescence excitation block (1), multichannel photodetector (2) and computer (3).

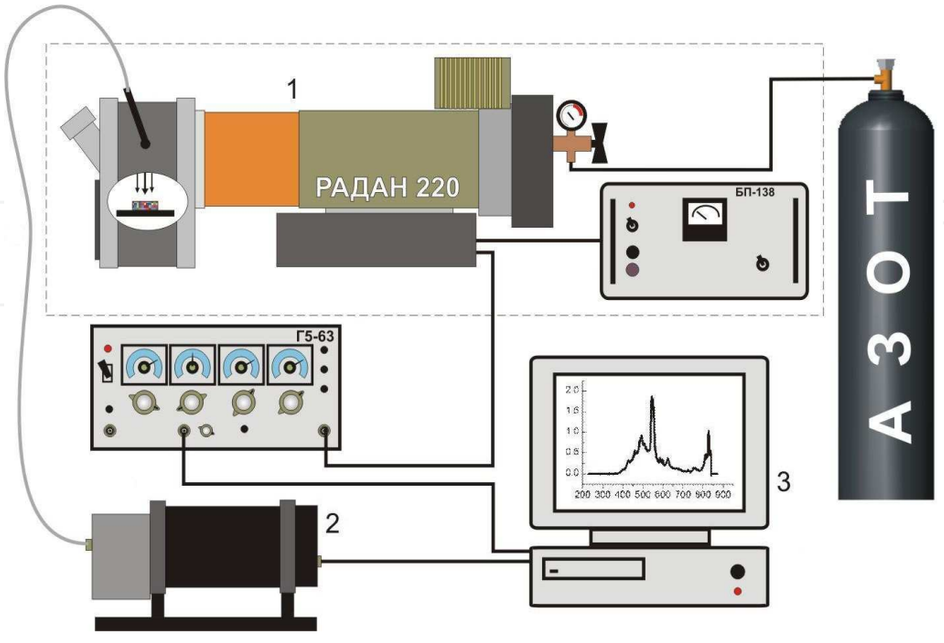

Fig. 2. Scheme of experimental setup

The excitation block (1) represents a combination of RADAN-220 pulsed electron accelerator and analytical chamber. The operating principle of the accelerator is based on the explosive emission of electrons from the cold cathode of accelerating tube. The RADAN-220 generates electron beam with the duration of 2 ns. The voltage that can be applied to the accelerating tube ranges from 150 to 220 keV. The commercially available IMA3-150E tube is placed in the analytic chamber. The generated electron beam is extracted to air through the beryllium foil and directed vertically downwards. The luminescence stream is transferred to the multichannel photodetector (2) by means of the silica multifiber. Computer (3) is the control system of the experimental setup. "Specad" software makes possible to realize various modes of the photodetector. It provides the calibration, registration, reviewing, processing and archiving of obtained spectra. The commercially available pulsed cathodoluminescent spectrograph "CLAVI" [Michailov et. al., 2001] was created on basis of this experimental setup.

3. The application of the pulsed cathodoluminescence for the luminescent analysis of $Nd^{3+}:Y_3Al_5O_{12}$ and $Nd^{3+}:Y_2O_3$

In the last year the intensive investigations in the field of the optical ceramics creation based on the metal refractory oxide doped with rare-earth ions, particularly $Nd^{3+}:Y_3Al_5O_{12}$ и $Nd^{3+}:Y_2O_3$ are carried out [Ikesue et. al., 1995, Lu et. al., 2001, Bagaev et. al., 2009]. The advantages of the laser ceramics against single crystals include the possibility of creating multilayer elements with sizes greater than those of single crystals, larger concentration of active ions, and lower manufacturing cost. The fitness of crystals or ceramics for active laser elements is determined usually by the photoluminescent methods in infrared region by means of lifetime measurement of upper laser Nd ion level $^4F_{3/2}$ [Hoskins et. al., 1963, Lupei et. al., 1995]. For this aim the method is effective, however it doesn't display couses of the lifetime decrease of the laser level. This is necessary to know to correct the conditions the conditions of crystal and ceramics synthesis of synthesis of crystalls and ceramics. Below the investigation of the PCL spectra is given. The possibility of realization of qualitative and quantitative luminescent analyses of $Nd^{3+}:Y_3Al_5O_{12}$, $Nd^{3+}:Y_2O_3$ laser materials is developed.

3.1 The luminescence of $Nd^{3+}:Y_3Al_5O_{12}$

The emission lines of neodymium ions in $Nd^{3+}:Y_3Al_5O_{12}$ in visible range correspond to the transitions from $4f^25d^1\ ^2F2_{5/2}$ level, which has three Stark components ν_0=37775 cm^{-1}, ν_1=37864 cm^{-1}, ν_2=38153 cm^{-1}, to the levels of $4f^3$ configuration of neodymium ion [Kolomiycev et. al., 1984]. The wavelengths of observed luminescent lines and their identification for $Nd^{3+}:Y_3Al_5O_{12}$ single crystal are presented in Table 1 in the first and the second columns, respectively. The numbers of Stark sublevels in according to nomenclature [Koningstein et. al., 1964] at increasing their energy, starting with zero, are pointed next to symbol of electron level in brackets; then emission band wavelengths, presented in [Kolomiycev et. al., 1982], are shown in brackets.

A conspicuous difference appears in PCL spectra of neodymium ions in yttrium aluminates in case of different crystal structure. The spectrum of orthorhombic $Nd^{3+}:YAlO_3$ single crystal together with the spectrum of cubic $Nd^{3+}:Y_3Al_5O_{12}$ are presented in Fig. 3 as an illustration of this difference.

$Nd^{3+}:Y_3Al_5O_{12}$		$Nd^{3+}:YAlO_3$	
λ, nm	Identification of optical trasfer	λ, nm	Identification of optical trasfer
		389,9	$^2F2_{5/2}$ (2)→$^2H_{9/2}$ (0), (390,0)
		394,6	$^2F2_{5/2}$ (0)→$^4F_{5/2}$ (2), (394,6)
399,2	$^2F2_{5/2}$ (0)→$^2H_{9/2}$ (2), (397,5)	398,1	$^2F2_{5/2}$ (0)→$^2H_{9/2}$ (3), (398,3)
401,6	$^2F2_{5/2}$ (0)→$^2H_{9/2}$ (4), (401,4)		
		422,5	$^2D_{5/2}$ (2)→$^4I_{9/2}$ (1), (423,0)
		426,9	$^2F2_{5/2}$ (2)→$^4F_{9/2}$ (3), (427,3)
429,9	$^2F2_{5/2}$ (1)→$^4F_{9/2}$ (0), (430,2)	429,9	$^2F2_{5/2}$ (1)→$^4F_{9/2}$ (0), (429,9)
435,6	$^2F2_{5/2}$ (0)→$^4F_{9/2}$ (2), (435,1)	435,2	$^2F2_{5/2}$ (1)→$^4F_{9/2}$ (1), (434,8)
		439,0	$^2D_{5/2}$ (0)→$^4I_{9/2}$ (4), (438,8)
		440,7	$^2P_{1/2}$ (0)→ $^4I_{9/2}$ (3), (441,2)
450,4	$^2F2_{5/2}$ (2)→$^2H_{11/2}$ (3), (450,5)	450,4	$^2F2_{5/2}$ (2)→$^2H_{11/2}$ (3), (450,4)
455,4	$^2F2_{5/2}$ (0)→$^2H_{11/2}$ (1), (455,9)	456,0	$^2F2_{5/2}$ (1)→$^2H_{11/2}$ (3), (456,0)
458,8	$^2F2_{5/2}$ (0)→$^2H_{11/2}$ (3), (458,3)		
461,0	$^2F2_{5/2}$ (0)→$^2H_{11/2}$ (4), (461,4)		
479,3	$^2F2_{5/2}$ (1)→$^4G_{5/2}$ (1), (479,0)	480,7	$^2F2_{5/2}$ (1)→$^4G_{5/2}$ (2), (480,5)
487,5	$^2F2_{5/2}$ (0)→$^2G_{7/2}$ (0), (487,1)	487,8	$^2F2_{5/2}$ (0)→$^2G_{7/2}$ (2) (488,1)
494,4	$^4G_{11/2}$ (2)→$^4I_{9/2}$ (4) (494,2)		
525,2	$^2F2_{5/2}$ (0)→$^4G_{7/2}$ (0), (524,9)	525,4	$^2F2_{5/2}$ (1)→$^4G_{7/2}$ (1), (525,4)
		527,8	$^2F2_{5/2}$ (1)→$^4G_{7/2}$ (2), (527,8)
		538,0	$^2F2_{5/2}$ (1)→$^4G_{9/2}$ (2), (538,3)
540,6	$^2F2_{5/2}$ (0)→$^2K_{13/2}$+$^2G_{9/2}$ (2), (541,0)	539,5	$^2F2_{5/2}$ (0)→$^4G_{9/2}$ (0), (539,3)
		541,6	$^2F2_{5/2}$ (2)→$^2K_{13/2}$ (2), (542,0)
		545,7	$^2F2_{5/2}$ (2)→$^2K_{13/2}$ (4), (545,7)
		547,5	$^2F2_{5/2}$ (2)→$^2K_{13/2}$ (5), (547,5)
549,1	$^2F2_{5/2}$ (0)→$^2K_{13/2}$+$^2G_{9/2}$ (7), (549,4)	549,2	$^2F2_{5/2}$ (0)→$^2K_{13/2}$ (0), (549,0)
		554,5	$^2F2_{5/2}$ (0)→$^2K_{13/2}$ (3), (554,2)
		556,3	$^2F2_{5/2}$ (0)→$^2K_{13/2}$ (4), (556,2)
557,4	$^2F2_{5/2}$ (0)→$^2K_{13/2}$+$^2G_{9/2}$ (10),(557,0)		
562,9	$^2K_{15/2}$ (3)→$^4I_{13/2}$ (0), (562,6)	563,6	$^2K_{13/2}$ (4)→$^4I_{11/2}$(1), (563,5)
576,4	Superposition $^2G_{7/2}$ (2,3)→$^4I_{9/2}$ (0,2), (576,3)		
		585,4	$^2F2_{5/2}$ (2)→$^4G_{9/2}$ (4), (585,2)
587,4	$^2F2_{5/2}$ (0)→$^4G_{9/2}$ (0), (586,8)		
596,2	Superposition $^2F2_{5/2}$ (0)→$^4G_{11/2}$ (0,1), (596,2)		
600,6	$^2F2_{5/2}$ (0)→$^4G_{11/2}$ (3), (600,1)		
		602,1	$^2F2_{5/2}$(2)→$^4G_{11/2}$+$^2K_{15/2}$+$^2D_{3/2}$(6),(601,8)
		610,4	$^2F2_{5/2}$(0)→$^4G_{11/2}$+$^2K_{15/2}$+$^2D_{3/2}$(4),(610,2)
		612,1	$^2F2_{5/2}$(1)→$^4G_{11/2}$+$^2K_{15/2}$+$^2D_{3/2}$(6),(611,8)
		615,4	$^2F2_{5/2}$(2)→$^4G_{11/2}$+$^2K_{15/2}$+$^2D_{3/2}$(13),(614,7)
620,1	$^2F2_{5/2}$ (0)→$^2K_{15/2}$ (2), (620,8)	620,1	$^2F2_{5/2}$(0)→$^4G_{11/2}$+$^2K_{15/2}$+$^2D_{3/2}$(9),(619,8)
		622,1	$^2F2_{5/2}$(1)→$^4G_{11/2}$+$^2K_{15/2}$+$^2D_{3/2}$(11),(621,4)
		625,4	$^2F2_{5/2}$(1)→$^4G_{11/2}$+$^2K_{15/2}$+$^2D_{3/2}$(13),(625,2)
		638,3	$^2H_{11/2}$ (1)→$^4I_{9/2}$ (2) (637,7)
		639,5	$^2H_{11/2}$ (0)→$^4I_{9/2}$ (2) (639,1)
		646,2	$^2H_{11/2}$ (3)→$^4I_{9/2}$ (3) (645,4)
		652,4	$^2H_{11/2}$ (3)→$^4I_{9/2}$ (4) (652,6)
		660,9	$^2G_{7/2}$ (3)→$^4I_{11/2}$ (4) (660,8)
		665,3	$^2G_{7/2}$ (0)→$^4I_{11/2}$ (3) (665,3)
		668,6	$^2G_{7/2}$ (0)→$^4I_{11/2}$ (4) (667,9)

Table 1. PCL lines and their identification for $Nd^{3+}:Y_3Al_5O_{12}$ and $Nd^{3+}:YAlO_3$ single crystals

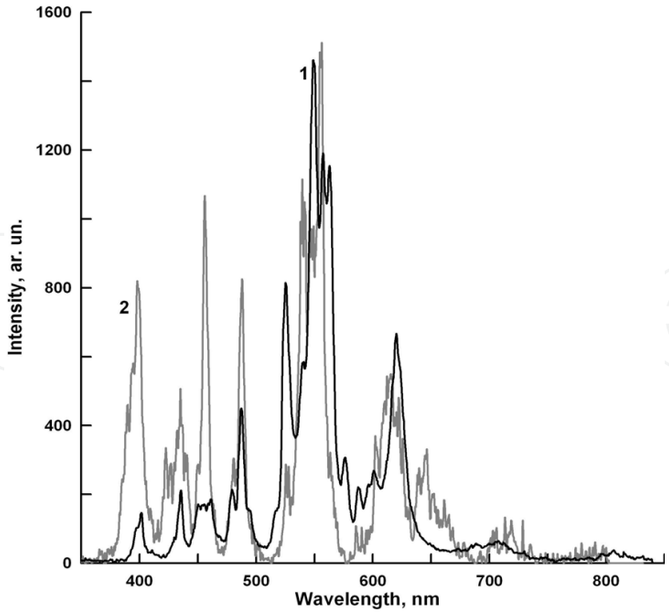

Fig. 3. The PCL spectra of $Nd^{3+}:Y_3Al_5O_{12}$ (1) and $Nd^{3+}:YAlO_3$ (2) single crystals

The wavelengths of fundamental neodymium luminescent lines and their identification for $Nd^{3+}:YAlO_3$ single crystal are presented in Table 1 in the third and the fourth columns, respectively [Osipov et. al., 2011].

The Fig. 3 and Table 1 show that the principal change is manifested in the considerable increase of the luminescent band numbers in the yttrium monoaluminate spectrum. This takes place due to activation of d-f transitions between the different Stark sublevels and the appearance of f-f transitions. These changes arise from the distortion of crystalline field symmetry in positions of individual neodymium ions that leads to the modifications of the oscillator strength and optical transition probability. Thus, the distortion of crystalline field symmetry appears in the spectrum as the change in intensity and numbers of emission bands.

The differences in the spectra can be used for the determination of the second phase content in $Nd^{3+}:Y_3Al_5O_{12}$ [Osipov et. al., 2011]. The luminescence lightsum in the spectrum region from λ_1 to λ_2 ($S = \int_{\lambda_1}^{\lambda_2} I(\lambda)d\lambda$) can be presented by the additive function depended from the dominant phase content C_g (cubic $Nd^{3+}:Y_3Al_5O_{12}$) and the second phase C_{im}=1-C_g

$$S = \alpha \cdot C_g + \beta \cdot (1 - C_g), \tag{8}$$

where α and β are the coefficients of proportionality. They are determined by the integration range and excitation conditions. To eliminate the influence of the intensity instability it is necessary to use the ratio of lightsums (S_1/S_2) as the analytical parameter calculated for two ranges of the spectrum. The lightsums in the ranges 350-500 nm (S_1) and 501-650 nm (S_2) to obtain the functional relation between the C_g and the luminescence intensity of neodymium ions have been chosen. In that case in accordance with Eq. (8) the content of cubic phase into $Nd^{3+}:Y_3Al_5O_{12}$ is defined the following equation

$$C_g = \frac{\beta_1 - \beta_2 \, S_1/S_2}{(\alpha_2 - \beta_2) S_1/S_2 - (\alpha_1 - \beta_2)} \tag{9}$$

In Fig. 4 the correlation between the C_g and S_1/S_2, calculated for the samples with known content of cubic phase is shown.

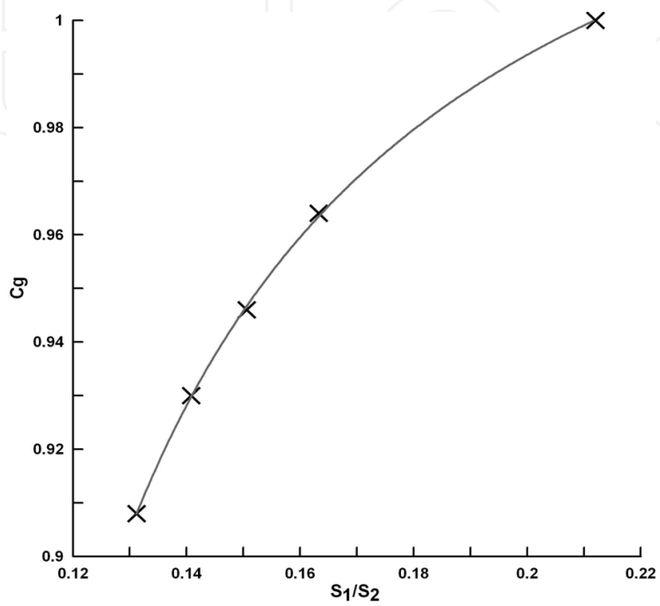

Fig. 4. The correlation between the C_g and S_1/S_2.

This dependence (Fig. 4) is approximated by the following equation with the $r^2>0.99$

$$C_g = \frac{1.071 \cdot S_1/S_2 - 0.084}{S_1/S_2 - 0.069}. \tag{10}$$

Moreover the obtained data validity was checked out by the analysis of samples with electron and optical microscopes.

3.2 The luminescence of Y_2O_3, Nd^{3+}:Y_2O_3

The wide band of intrinsic radiation in visible range is a visiting luminescent card of pure yttria. Earlier the other authors observed this band at different excitation type [Conor, 1964, Kuznetsov et. al., 1978, Bordun et. al., 1995]. Even at cryogenic temperature of the samples the unresolved band was registered.

We investigated commercially available yttria powders with a particle sizes of 1-3 μm and 5-10 μm. All the powders have a cubic lattice of the α-Y_2O_3. From these commercial powders, nanopowders with the average particle size of 10-12 nm were prepared by the laser evaporation method. Particles were crystallized in the metastable monoclinic phase γ-Y_2O_3. After annealing they transformed to the α-Y_2O_3.

The spectrum of the powder with particle size of 1-3 μm has a broad asymetric band peaked at 437 nm and long – wavelength wing shows local maxima (Fig. 5, curve 1).

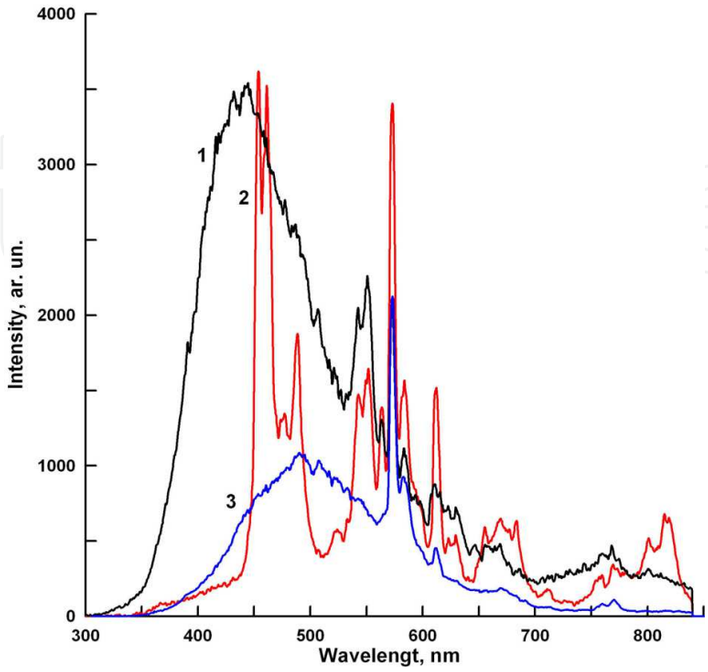

Fig. 5. PCL spectra of commercial yttria powders with particle size 1-3 μm (1), 5-10 μm (2) and nanopowders with the average particle size of 10-12 nm (3).

In the spectrum of the powder with the particle size of 5-10 μm almost all local maxima are transformed into narrow bands (Fig. 5, curve 2). They are grouped into four series 435 – 510 nm (the blue series), 515 – 640 nm (the orange series), 645 – 700 nm (the red series) and 785 – 840 nm (the infrared series). The PCL spectra of nanopowders, irrespective of the crystal phase (either the γ-Y_2O_3 or the α-Y_2O_3 phase) and of the initial coarse powder, have a similar structures (Fig. 3, curve 3). The broad band with the maximum at 485 nm dominates in these spectra. The peak range of this band exhibits local maxima of the blue series. Also the lines of orange series at 573, 583, 612 nm become apparent. The red series is weak, while the infrared series is hardly seen.

The range of the band series observed in the spectra of pulsed cathodoluminescence corresponds to the range of intrinsic radiation of yttria, which is identified as the radiation of associated donor-acceptor pairs Y^{3+} - O^{2-} [Bordun, 2002].

Since the luminescence wavelengths of narrow bands of commercial powders, nanopowders coincide, we can assume that these materials contain intrinsic luminescence centers of the same type.

The series of PCL bands of yttria resemble the radiation of free YO radicals, which is observed, for example, in laser plume of yttria-containing target [Osipov et. al., 2005]. This radical has been fairly well studied [Pearse et. al., 1949]. The Table 2 shows the wavelengths of the bands observed in PCL spectra and their identification. In the second column of this table the wavelengths of the strongest bands are in boldface.

Intrinsic luminescence center	
V′→V″	**λ, nm**
Blue band series, the electronic transition $B^2\Sigma \rightarrow X^2\Sigma$	
0→0	**453.8**
2→2	458.6
3→3	**461.1**
0→1	470.6
2→3	475.2
0→2	**488.7**
Orange band series, the electronic transition $A^2\Pi \rightarrow X^2\Sigma$	
$2\rightarrow0+(T_g+A_g)=380$	**542.8**
1→0	**551.6**
$1\rightarrow0+(T_g+A_g)=380$	**563.5**
0→0	**572.9**
3→3	**583.6**
0→1	600.0
3→4	**612.2**
0→2	629.3
Red band series, the electronic transition $A^2\Pi \rightarrow X^2\Sigma$	
$0\rightarrow3-(T_g+A_g)=162$	655.3
0→3	662.4
$0\rightarrow3+(T_g+A_g)=162$	669.6
$0\rightarrow3+T_g=469$	683.8
Infrared band series, the electronic transition $A^2\Pi \rightarrow X^2\Sigma$	
$0\rightarrow5+(T_g+A_g)=380$	760.8
0→6	785.0
	801.1
	818.4

Table 2. Parameters of the PCL lines in the yttria spectrum

Based on these data, we constructed the energy scheme of the intrinsic luminescence center (Fig. 6). Qualitatively this scheme coincides with that of the YO free radicals. In this scheme the configuration curves were calculated in the harmonic oscilator approximation as

$$E_i = E_{0i} + \frac{2\pi^2 c\nu_i m_0}{h} \cdot 10^{-16}(r-\rho_i)^2 , \tag{11}$$

where i =X, A and B denotes the electronic states $X^2\Sigma$, $A^2\Pi$, and $B^2\Sigma$, E_{0i}, ρ_I, and ν_i are the minimal energy, the equilibrium distance, and the wavenumber of the vibration mode of i^{th} electronic state, respectively; m_0 is the mass of the oxygen atom; c and h are the light speed and Planck's constant. The energy E and wavenumbers ν_i are expressed in (11) in reciprocal centimetres, the amplitudes of the $(r-\rho_i)$ vibrations are given in nanometres.

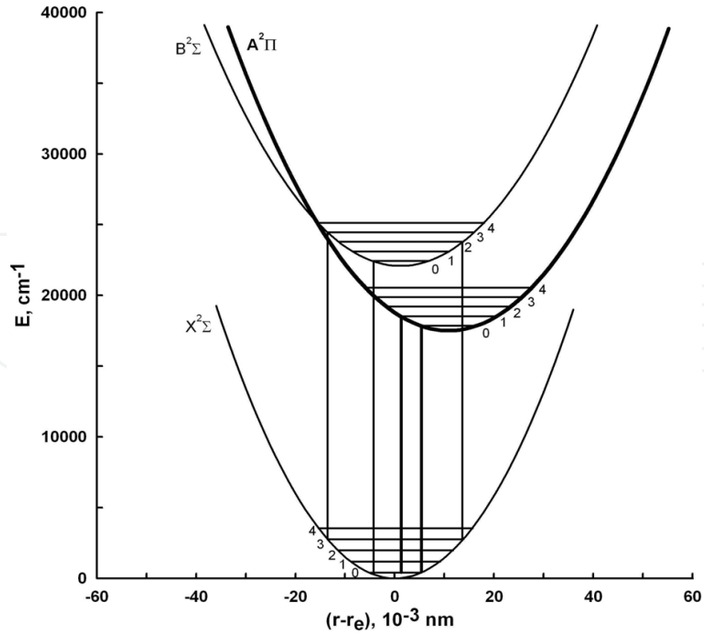

Fig. 6. Energy scheme of the intrinsic luminescence center

For the configuration curves of the $X^2\Sigma$, $A^2\Pi$, and $B^2\Sigma$ states (Fig. 6) E_{0i}=0, 17510, and 22090 cm^{-1} and ν_i=786, 675, and 675 cm^{-1}, respectively. With these parameters, up to the measurement error, the wavelengths of pulsed cathodoluminescence coincide with the wavelengths of the optical transitions shown in Table 2. The Franck – Condon principle for molecular transitions is most precisely implemented at $\rho_A=\rho_X+10.8709\cdot10^{-3}$ nm and $\rho_B=\rho_X+1.2351\cdot10^{-3}$ nm, and ρ_X can be estimated as half of elementary cube edge, ρ_X=0.1385 nm. For electronic – vibration transitions for which one of the vibration quantum numbers V is large, this principle is implemented only if these transitions involve the most strong phonons [Schaak et. al., 1970], Table 2. Under these parameters, the configuration curves of the electronic states $A^2\Pi$ and $B^2\Sigma$ intersect at the point with E=25256 cm^{-1}.

The qualitative coincidence of the emission bands and the energy structure of intrinsic luminescence centres observed by us and YO free radicals allow us to conclude that intrinsic luminescence centres in yttria contain bound YO radicals [Osipov et. al., 2008]. Consider the possibility of formation of such intrinsic luminescence centre. It is known [Schaak et. al., 1970] that the cubic yttria has unit cell composed of 16 formula units Y_2O_3. Twenty four cations occupy positions with C_2 symmetry and eight cations occupy the positions with C_{3i} symmetry (Fig. 7). Every cation is surrounded by six oxygen ions which are positioned on the corners of deformed cube with the edge size of 0.2702 nm, at that two corners is unoccupied. Thus in one-third of the cubes (YO_6) two oxygen vacancies are located at the cube corners along the face diagonal, while, in the remaining cubes, they are located along the body diagonal (Fig. 7).

For such packing a structure, presented in Fig. 8. ,can be formed at the outer cube face that contains two oxygen vacancies and that is located at the crystal boundary. In essence, this structure is the YO radical bound to the crystal lattice by the yttriun ion. On such surfaces the fraction of faces with two oxygen vacancies is 1/3×1/6=1/18 and the average distance

between them is about 5 nm. All of this leads to the dependence of the luminescence spectrum of such bound radicals on the particle size of yttria mainly via their shape.

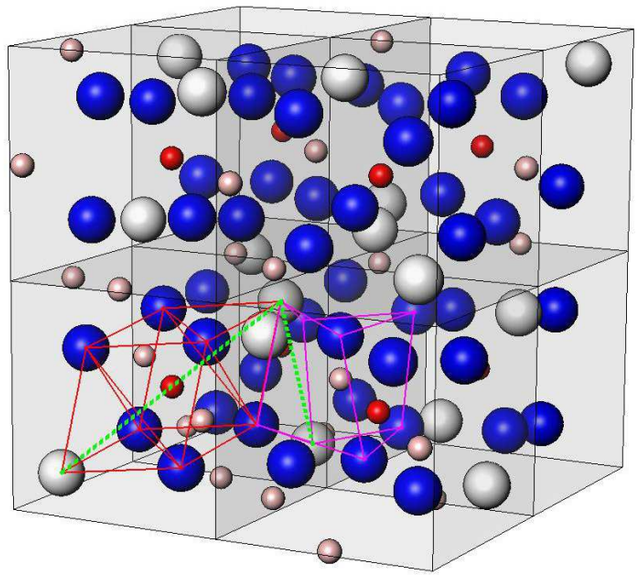

Fig. 7. The unit cell of yttria. The yttrium positions with C_{3i} and C_2 symmetry designated by red and pink balls respectively. The oxygen and the vacant positions designated by blue and grey balls. The vacant positions are associated by green dot line.

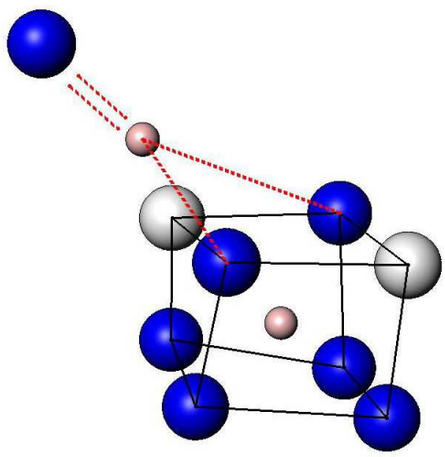

Fig. 8. The structure of intrinsic luminescence centre.

The considered above intrinsic luminescence centre also presents in Nd^{3+}:Y_2O_3. However the presence of neodymium results in decrease of the intrinsic band intensity and distortion of its profile. We studied the monoclinic and cubic Nd^{3+}:Y_2O_3 nanopowders. The nanopowders were prepared using a mixture of micropowder α-Y_2O_3 phase and 1 mol.% Nd_2O_3 powder. After evaporation of this mixture by CO_2 laser Nd^{3+}:Y_2O_3 nanoparticles were crystallized into monoclinic phase. To transfer nanopowders into cubic phase annealing in air was carried out above 900°C [Kotov et. al., 2002].

The PCL spectra of all Nd^{3+}:Y_2O_3 samples contain emission lines of neodymium ions, which have not been previously observed in photoluminescence. Namely, neodymium doped nanopowders exhibit a strong band peaking at 825 nm (Fig. 9).

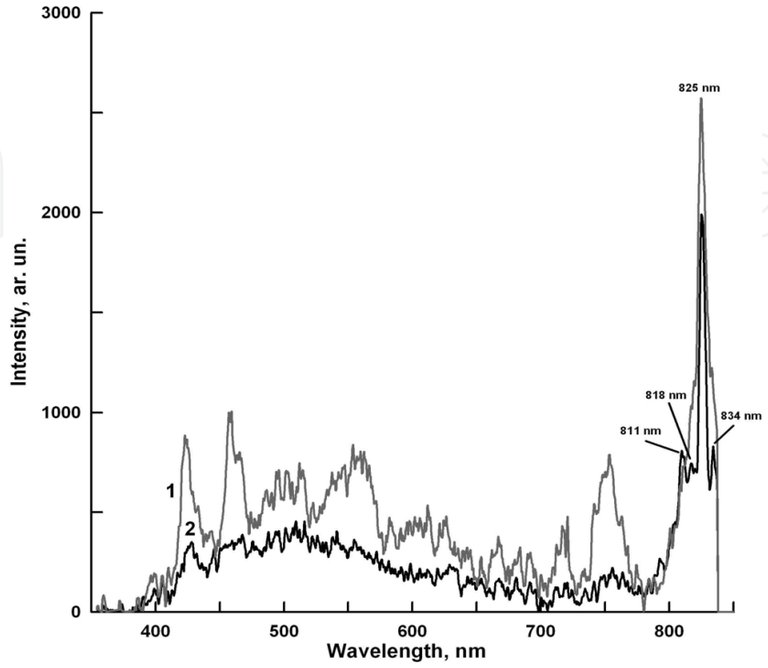

Fig. 9. The PCL spectra of monoclinic (1) and cubic (2) Nd^{3+}:Y_2O_3 nanopowders

Its components correspond well to the $^4F_{5/2}\rightarrow{}^4I_{9/2}$ (825, 811, 834 nm) and $^2H_{9/2}\rightarrow{}^4I_{9/2}$ (818 nm) optical transitions between Nd^{3+} Stark's sublevels with the energies in Y_2O_3 cubic lattice [Chang, 1966]. These components are resolved only in cubic samples (Fig. 9). Therefore the splitting of Stark's components allows us to conclude about the presence of the dominant phase into Nd^{3+}:Y_2O_3.

To check this assumption the additional investigations were made. In Fig 10. the PCL spectra of pressed nanopowders (compacts) are presented. The compacts were annealed at 530, 750, 950, 1100, and 1300°C. The X-ray analysis for this samples showed that the unannealed compact and annealed compact at 530°C have monoclinic phase, all remaining compacts are cubic samples. It is shown that the splitting of neodymium band at region of 800-840 nm only takes place in cubic samples and one component appears at 825 nm in monoclinic samples.

In addition to the band in the region of 800-840 nm two emission bands of neodymium ions arise in the Nd^{3+}:Y_2O_3. These are a weak band at 720 nm due to $^4F_{9/2}\rightarrow{}^4I_{9/2}$ transition and stronger band at 750 nm with the components due to the transitions between the Stark sublevels: $^4F_{7/2}\rightarrow{}^4I_{9/2}$ and $^4S_{3/2}\rightarrow{}^4I_{9/2}$.

The intensity weaking of intrinsic band into Nd^{3+}:Y_2O_3 is associated with the quantitative decrease of this centres, since the part of yttrium ions are replaced by the neodymium ions. The distortion of the intrinsic band is determined by the neodymium absorption of it. The most absorption is observed in region at 560-613 nm [Osipov et. al., 2009].

In addition to the present bands into Nd^{3+}:Y_2O_3 the appearance of four well-resolved components in the range of 610-660 nm can be seen. The specta of this band for compacts annealed at 950 and 1300°C are presented in Fig. 11. The band contains the following four narrow lines at 620.6, 630.6, 645.3, 655.6 nm which we identify using Raman spectra, as luminescence of oxygen molecular ion O_2^- [Solomonov et. al., 2011].

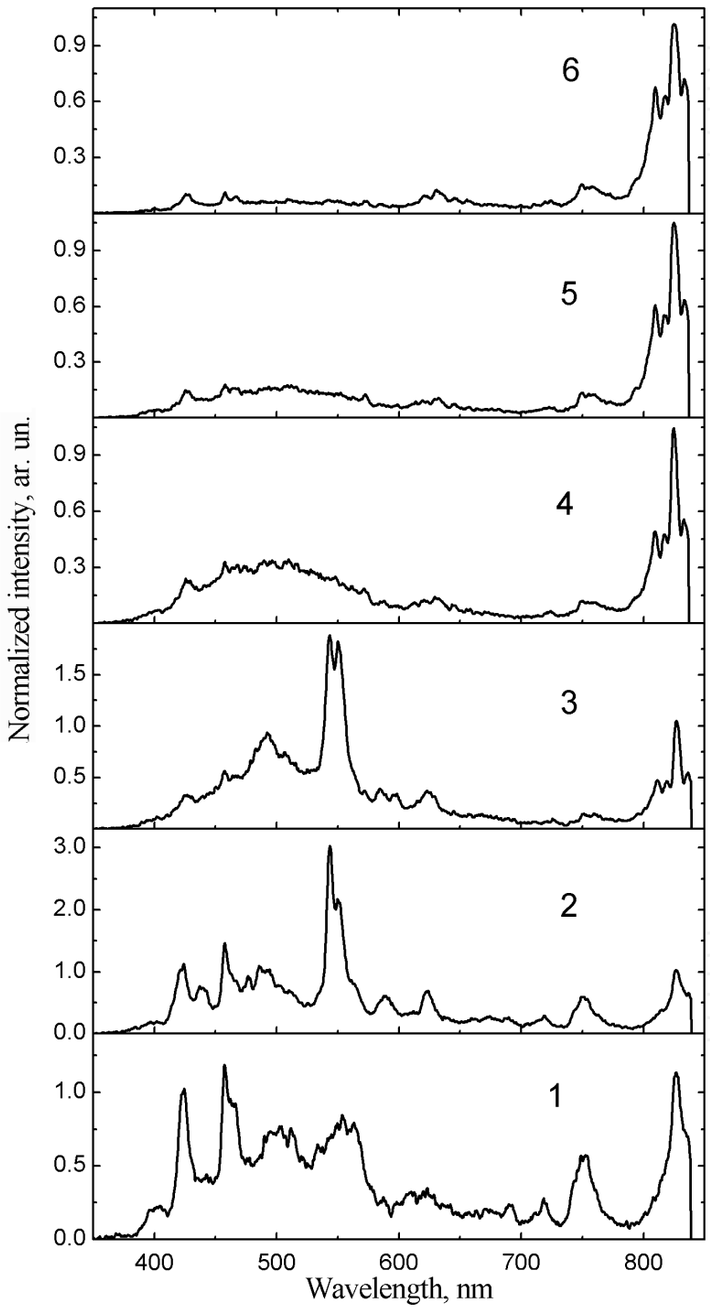

Fig. 10. The PCL spectra of unannealed compact (1) and compacts annealed at 530°C (2), 750°C (3), 950°C (4), 1100°C (5), 1300°C (6).

The bands with the frequencies of 1615 and 1702 cm^{-1} correspond to vibrations of the molecular ion in the ground state, while the frequencies at 966 and 993 cm^{-1} correspond to the excited state for the two sites of the oxygen molecular ion in the yttria lattice.

Fig. 12 demonstrates two sites of defects O_2^- taking into account the occurrence of two types of natural vacancies about we talked earlier.

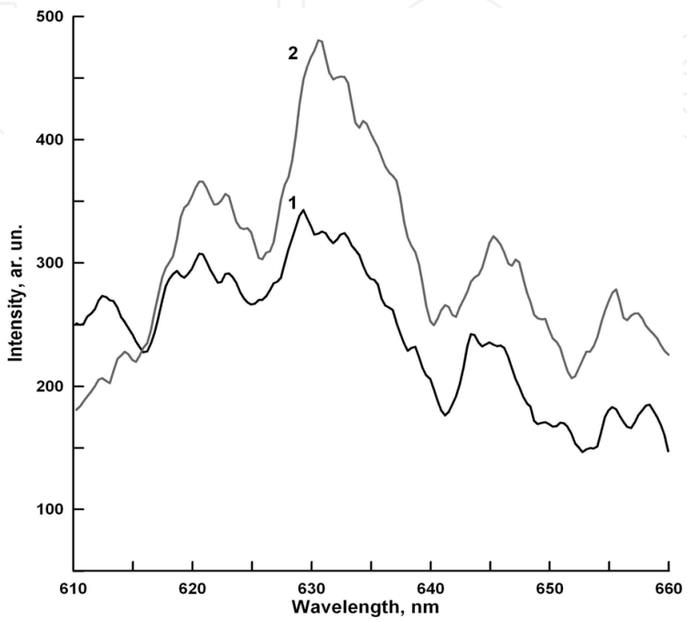

Fig. 11. The PCL of oxygen molecular ions.

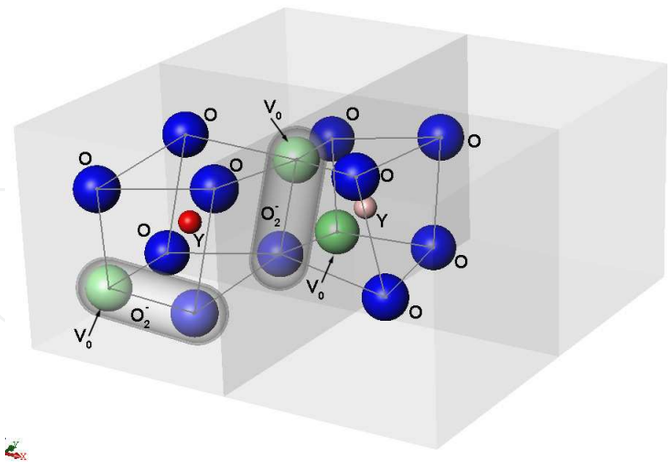

Fig. 12. Two sites of oxygen molecular ions defects in lattice of cubic Y_2O_3

Fig. 13 presents two potentional curves and formation of luminescence bands. The lowest excited state $A^2\Pi_u$ of the oxygen molecular ion can be stabilized.

The observed luminescence band results of the transition from the vibration level V′=0 of the excited electronic state $A^2\Pi_u$ to one vibration level V′′=3 of the ground state $X^2\Pi_g$. The

bands at 630.6 and 655.6 nm are formed due to the transition to the vibration level of the groun state with the participation of lattice phonons. For the first curve the phonon energy is 255 cm, while, for the second curve it is 244 cm^{-1}. These phonons are observed in the Raman spectrum. The excited electronic state of the molecular ion is spaced from the ground state by 20660-21580 cm^{-1} [Solomonov et. al., 2011].

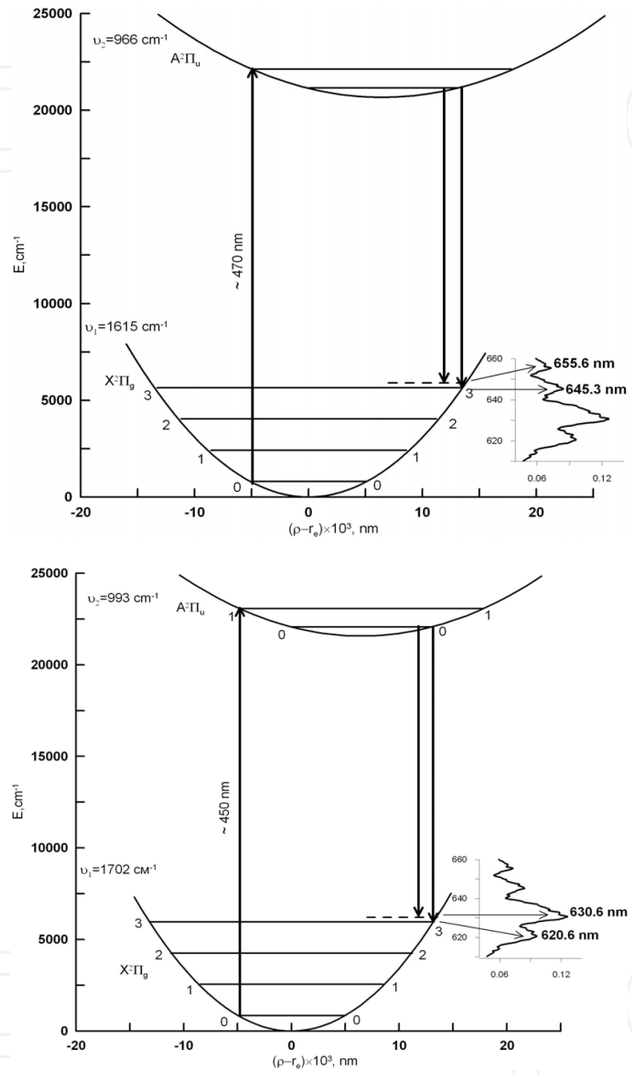

Fig. 13. Configuration curves for two sites of oxygen molecular ions

On the basis of the qualitative luminescent analysis of $Nd^{3+}:Y_2O_3$ the determination of neodymium concentration by means of the calibration curve construction is possible because of intensity of neodymium lines is proportional to it concentration $I_{Nd}(\lambda_i)=a_i \cdot C_{Nd}$ (for example 750 or 825 nm). However we can't use this equation because PCL spectrum is characterized by the instability. Therefore we also chose lightsums ratio as analytic parameter in regions of 730-840 nm and 350-840 nm. The first region of $Nd^{3+}:Y_2O_3$ spectrum involves only neodymium bands, but the second one includes in addition the intrinsic band which is distorted by the neodymium absorption and can be ascribed as follows

$$I_{YO}(\lambda_i) = I_{0i}\frac{1-\exp(-k_i \cdot C_{Nd} \cdot l)}{k_i \cdot C_{Nd}} \tag{12}$$

Here I_{0i}, l, k_i are the intensity of i – intrinsic band without absorption, the thickness of samples, coefficient of absorption of i – band, respectively. Hence relation of lightsums ratio (S(350-840)/S(730-840)) with C_{Nd} has to include the equation (12). Really this relation is decribed by the following equation

$$\frac{S(350-840)}{S(730-840)} = A \cdot \frac{1-\exp(-B \cdot C_{Nd})}{C_{Nd}^2} + D. \tag{13}$$

Fig. 14 demonstrates the calibration curve (r^2>0.99) for the determination of neodymium concentration in region of 0.11 – 1.07 at. %.

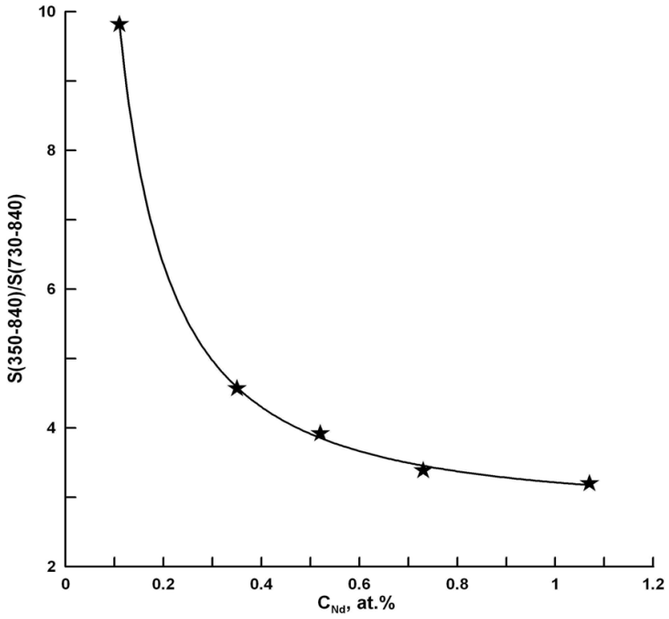

Fig. 14. The calibration curve for the determination of neodymium concentration in region of 0.11 – 1.07 at. %.

4. Conclusion

Thus, the possibility of realization of rapid, nondestructive, qualitative and quantitative luminescent analyses of laser materials, in particular Nd^{3+}:$Y_3Al_5O_{12}$, Nd^{3+}:Y_2O_3, with the help of pulsed cathodoluminescence was shown.

5. References

Bagaev, S.; Osipov, V.; Ivanov, M.; Solomonov, V.; Platonov, V.; Orlov, A.; Rasuleva, A. & Vatnik, S. (2009).Fabrication and characteristics of neodymium – activated yttrium oxide optical ceramics. *Optical Materials,* Vol.31, pp. 740-743, ISSN 0925-3467

Bogdankevich, O.; Darznik, S. & Eliseev, P. (1975). *Semiconductor lasers,* Nauka, Moscow, Russia

Bordun, O.; Bordun, I. & Novosad, S. (1995). Luminescence centres into Y_2O_3. *Journal of applied spectroscopy,* Vol.62, No.6, pp. 91-95, ISSN 0021-9037

Bordun, O. (2002). Influence of oxygen vacancies on the luminescence spectra of thin Y_2O_3 films. *Journal of applied spectroscopy,* Vol.69, No.3, pp. 371-374, ISSN 0021-9037

Chang, N. (1966). Energy levels and crystal – field splittings of Nd^{3+} in yttrium oxide. *J. Chem. Phys.,* Vol.44, pp. 4044-4050, ISSN 0021-9606

Chukichev, M.; Sabri, D.; Sokolov, V. & Surcova T. (1990). Cathodoluminescence of solid solution $Zn_{1-x}Mn_xSe$. *Optics and Spectroscopy,* Vol.68, pp. 2000-2021, ISSN 0030-4034

Connor, O. (1964). A theory of thermoluminescence of fluorite (CaF_2:Y). Radiative recombination from highly associated electron – hole pairs. *Appl. Phys. Lett.,* Vol.4, No.1, pp. 126-129, ISSN 0003-6951

Galkin, G. (1981). The interband processes of the recombination into semiconductors at high excitation level. *Proceedings of the P.N. Lebedev Physical Institute (Trudi FIAN),* Vol.128, pp. 3-64

Hoskins, H. & Soffer, B. (1963). Stimulated emission from $Y_2O_3:Nd^{3+}$. *Appl. Phys. Lett.,* Vol.4, pp. 22-23, ISSN 0003-6951

Ikesue, A.; Kinoshita, T.; Kamata, K. & Yoshida, K. (1995). Fabrication and optical properties of high-performance polycrystalline Nd:YAG ceramics for solid-state lasers. *J. Amer. Ceram. Soc.,* Vol.78, pp. 1033-1040, ISSN 1551-2916

Kolomiycev, A.; Meylman, M.; Volodina, I.; Chukichev, M.; Smagin, A. & Bagdasarov H. (1982). Luminescence of neodymium – activated yttrium – aluminum garnet crystals in ultra-violet and visible ranges at high energy excitation. *Deposition in VINITI,* No. 5995-82, pp. 1-15.

Kolomiycev, A.; Meylman, M.; Volodina, I.; Chukichev, M.; Smagin, A. & Bagdasarov H. (1984). Luminescence of neodymium – activated yttrium – aluminum garnet crystals in ultra-violet and visible ranges at high energy excitation. *Optics and Spectroscopy,* Vol.56, pp. 365-367, ISSN 0030-4034

Koningstein, J. & Geusic, J. (1964).Energy levels and crystal – field calculations of neodymium in yttrium aluminum garnet. *Phys. Rev.,* Vol.136, No. 3A pp. 711-716, ISSN 1893-1912

Kotov, Yu.; Osipov, V.; Ivanov, M.; Samatov, O.; Platonov, V., Azarkevich, E.; Murzakayev, A. & Medvedev. A. (2002). Properties of oxide nanopowders prepared by target evaporation with a pulse – periodic CO_2 laser. *Technical Physics,* Vol.47, No.11 pp. 1420-1426, ISSN 1063-7842

Kuznetsov, A.; Abramov, V.; Rooze, N. & Savikhina, T. (1978). Autolocalized excitons into Y_2O_3. *JETP Letters,* Vol.28, No.10, pp. 602-605, ISSN 0021-3640

Lu, J.; Murai, T.; Takaichi, K.; Ueda, K.; Yagi, H.; Yanagitani, T. & Kaminskii, A. (2001) $Nd^{3+}:Y_2O_3$ ceramic laser. *Jpn. J. Appl. Phys.,* Vol.40, pp. 1277-1279, ISSN 0021-4922

Lupei, V.; Lupei, A.; Tiseanu, C.; Georgescu, S.; Stoicescu, C. & Nanau, P. (1995) High – resolution optical spectroscopy of YAG: Nd: A test for structural and distribution models. *Phys. Rev. B,* Vol.51, No.1 pp. 8-17, ISSN 0003-6951

Mesyats, G. (1974). *Generating of highpower nanosecond pulses,* The Soviet radio, Moscow, Russia

Mesyats, G.; Shpak, V.; Yalandin, M. & Shunailov S. (1992). Compact RADAN electron accelerators for testing new radiation technologies and sterilization. *Radiat. Phys. Chem.,* Vol.46, pp. 489-492, ISSN 0969-806X

Michailov, S.; Osipov, V. & Solomonov V. (2001). Pulsed cathodoluminescent analyzer of materials. *Pribory i tekhnika eksperimenta,* No.3, pp. 164-165, ISSN 0032-8162

Osipov, V.; Solomonov, V.; Platonov, V.; Snigireva, O.; Ivanov, V. & Lisenkov, V. (2005). Laser plume spectroscopy. 2. Graphite yttrium – stabilized and zirconium oxide targets. *Quantum Electron.,* Vol.35, No.7 pp. 633-637, ISSN 0368-7147

Osipov, V.; Rasuleva, A. & Solomonov, V. (2008). Luminescence of pure yttria. *Optics and Spectroscopy,* Vol.105, No.4 pp. 524-530, ISSN 0030-400X

Osipov, V.; Solomonov, V.; Spirina, A.; Ivanov, M. & Orlov, A. (2009). Luminescence of yttrium oxide doped with neodymium. *Optics and Spectroscopy,* Vol.106, No.1 pp. 78-83, ISSN 0030-400X

Osipov, V.; Solomonov, V. & Spirina, A. (2011). Luminescent investigation of neodymium doped yttrium aluminates. *J. of Optical Technology,* Vol.78, No.6 pp. 81-87, ISSN 0030-4042

Pearse, R. & Gaydon A. (1949). *The identification of molecular spectra,* Inostrannaya Literatura, Moscow, Russia

Petrov, V. (1996). Cathodoluminescent microscopy. *Physics - Uspekhi,* Vol.39, pp. 807-818, ISSN 0042-1294

Ramseyer, K.; Fisher, J.; Matter, A.; Eberhardt, P. & Geiss J. (1989). A cathodoluminescence microscope for low intensity luminescence. *Journal of Sedimentary Research,* Vol.59, pp. 619-622, ISSN 0022-4472

Ramseyer, K. & Millis J. (1990). Factors influencing short-lived blue cathodoluminescence in α - quartz. *Journal of Sedimentary Research,* Vol.59, pp. 619-622, ISSN 0003-004X

Schaak, G. & Koningstein, J. (1970). Phonon and electronic raman spectra of cubic rare-earth oxides and isomorphous ittrium oxide. *J. Opt. Soc. Amer.* Vol.60, No.8, pp. 1110-1115, ISSN 1551-2916

Solomonov, V. & Michailov, S. (2003). *Pulsed cathodoluminescence and its application for the analysis of condensed substances,* UB RAS, ISBN 5-7691-1357-X, Yekaterinburg, Russia

Solomonv, V. (2003). Kinetics of pulsed cathodoluminescence. *Optics and Spectroscopy,* Vol.95, pp. 248-254, ISSN 0030-4034

Solomonv, V.; Michailov, S; & Deykun, A. (1996). About the mecanism of excitation and the structure of the pulsed cathodoluminescence bands of Cr^{3+}, Mn^{2+} impurity ions into minerals. *Optics and Spectroscopy,* Vol.80, pp. 447-458, ISSN 0030-4034

Vaysburd, D.; Semin, B.; Tavanov, E.; Matlis, S.; Balichev, I. & Gering G. (1982) *Highenergy electronics of solid,* Nauka, Novosibirsk, Russia

Yang, B.; Luff, B. & Townsend F. (1992). Chatodoluminescence of natural zircons. *J. Phys.: Condens. Matter.,* Vol.4, pp. 5617-5624, ISSN 0953-8984

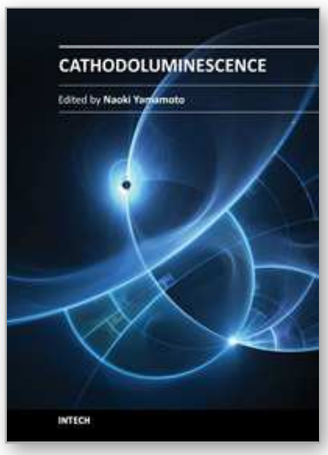

Cathodoluminescence

Edited by Dr. Naoki Yamamoto

ISBN 978-953-51-0362-2
Hard cover, 324 pages
Publisher InTech
Published online 28, March, 2012
Published in print edition March, 2012

Cathodoluminescence (CL) is a non-destructive technique to characterize optical and electronic properties of nanostructures in many kinds of materials. Major subject is to investigate basic parameters in semiconductors, impurities in oxides and phase determination of minerals. CL gives information on carrier concentration, diffusion length and life time of minority carriers in semiconductors, and impurity concentration and phase composition in composite materials. This book involves 13 chapters to present the basics in the CL technique and applications to particles, thin films and nanostructures in semiconductors, oxides and minerals. The chapters covered in this book include recent development of CL technique and applications to wide range of materials used in modern material science.

How to reference

In order to correctly reference this scholarly work, feel free to copy and paste the following:

Vladimir Solomonov and Alfiya Spirina (2012). What is the Pulsed Cathodoluminescence?, Cathodoluminescence, Dr. Naoki Yamamoto (Ed.), ISBN: 978-953-51-0362-2, InTech, Available from: http://www.intechopen.com/books/cathodoluminescence/what-is-the-pulsed-cathodoluminescence-

INTECH
open science | open minds

InTech Europe
University Campus STeP Ri
Slavka Krautzeka 83/A
51000 Rijeka, Croatia
Phone: +385 (51) 770 447
Fax: +385 (51) 686 166
www.intechopen.com

InTech China
Unit 405, Office Block, Hotel Equatorial Shanghai
No.65, Yan An Road (West), Shanghai, 200040, China
中国上海市延安西路65号上海国际贵都大饭店办公楼405单元
Phone: +86-21-62489820
Fax: +86-21-62489821

IntechOpen